Microsystem Technologies (2022) 28:1423–1434
https://doi.org/10.1007/s00542-019-04362-x

TECHNICAL PAPER

Analytical design of MEMS variable capacitors based on shaped-finger comb-drives

Dooyoung Hah[1]

Received: 28 August 2018 / Accepted: 19 February 2019 / Published online: 23 February 2019

Abstract
A variable capacitor is one of the widely used components in radio frequency (RF) circuits. Variable capacitors can benefit from the microelectromechanical systems (MEMS) technology, to be equipped with attractive characteristics such as high quality factor and wide tuning range. One of the design goals for MEMS varactors has been to realize linear capacitance–voltage (C–V) characteristics, for which a design method is proposed in this paper, based on shaped-finger comb-drive actuators. The shaped-finger design method, originally developed for a tunable optical filter application by the author, is redeveloped in this work for a linear C–V varactor. Moreover, the conformal mapping method is employed in calculation of capacitances, making the whole design process more time-efficient, being almost all-analytical with the minimum usage of numerical analysis methods. Effects of sense capacitor finger shapes to the optimized drive capacitor finger shapes and the corresponding C–V characteristics are investigated as well. Variable capacitors with the shaped-finger design show linearity factor (LF)—defined as the maximum deviation from the perfect linear relationship—as good as 0.4%, enormously improved from that of the conventional constant-finger-gap devices (LF: 49.9%). Further probed by 3-D numerical analysis, the C–V characteristics of the designed variable capacitor show LF better than 2.62% in the case of constant-gap sense capacitors, and as good as 0.77% in the case of shaped-finger sense capacitors. Versatility of the design method is further demonstrated by presenting a varactor for linear resonant frequency–voltage (f–V) characteristics in voltage-controlled oscillator (VCO) applications. Finally, effects of etch bias, one of common fabrication imperfections, to the linearity of C–V characteristics are studied. The developed analytical design method with shaped fingers can find a wide range of applications where comb-drive actuators are used.

1 Introduction

Variable capacitors have a wide range of uses in radio frequency (RF) circuits such as voltage-controlled oscillators (VCOs), impedance matching networks, tunable filters, phase shifters, and so on. Microelectro-mechanical systems (MEMS) technologies are attractive for variable capacitors, which can provide them with high quality factor and wide tuning ratio characteristics. Various control mechanisms have been used to tune capacitance, such as electrostatic (Dec and Suyama 2000; Yoon and Nguyen 2000; Seok et al. 2002; Abbaspour-Tamijani et al. 2003; Borwick et al. 2003; Xiao et al. 2003; Nguyen et al. 2004; Nieminen et al. 2004; Bakri-Kassem and Mansour 2009; Han et al. 2011; Elshurafa et al. 2012; Mahmoodnia and Ganji 2013; Afrang et al. 2015; Baek et al. 2015; Moreira et al. 2016; Pu et al. 2016; Baghelani and Ghavifekr 2017), electro-thermal (Feng et al. 2001; Reinke et al. 2010), piezoelectric (Kawakubo et al. 2006; Ikehashi et al. 2007), and so on. Among them, electrostatic control has been the most frequently adopted for its good compatibility with electronic circuits as well as low standing power consumption.

One of the design goals for the MEMS variable capacitor has been linear capacitance–voltage (C–V) characteristics, for which several groups made reports. One research group utilized a leverage mechanism to operate the parallel-plate type capacitor device in an increasing-gap mode instead of a typical closing-gap mode (Han et al. 2011). In another approach, a residual-stress-induced curved plate design was adopted in a gap-closing type device, achieving relatively linear but ragged C–V characteristics (Bakri-Kassem and Mansour 2009). Another research group incorporated an auxiliary fixed–fixed beam underneath a

✉ Dooyoung Hah
dooyoung.hah@agu.edu.tr

[1] Department of Electrical and Electronics Engineering, Abdullah Gül University, Kayseri, Turkey

gap-closing cantilever to modify the boundary condition, resulting in improved linearity overall, but with nontrivial local nonlinearity (Afrang et al. 2015). Another design combined vertical and horizontal variable capacitors so that fast increase in vertical capacitance is compensated by decrease in horizontal capacitance (Elshurafa et al. 2012).

In this paper, a new type of device is proposed for linear C–V characteristics, based on shaped-finger comb-drive actuators (Hah 2018b). Recently, the author reported a new design methodology with comb-drive actuators, by which linear wavelength-voltage characteristics were realized in tunable optical filters (Hah 2017, 2018a). In this method, comb finger shapes are calculated by solving a differential equation that models the optical and the electromechanical behaviors of the device. In this paper, the design method is modified to achieve linear C–V characteristics in variable capacitors. There also have been reports of shaped-finger comb-drive actuators by other research groups, where the finger shapes are calculated from straightforward, well-defined force profiles desired in each application by using either an optimization algorithm or a closed-form equation (Ye et al. 1998; Jensen et al. 2003; Lee et al. 2008; Engelen et al. 2010). In contrast to those approaches, the author's method is to find a solution to an application-specific objective equation which can be often complicated. For instance, the design can be modified once again to achieve linear resonant frequency–voltage (f–V) characteristics in VCO circuits. In the previous works reported for tunable optical filters (Hah 2017, 2018a), nontrivial efforts with numerical analysis were involved, especially in the capacitance calculation. The design method this paper reports, however, has become almost all-analytical by adopting conformal mapping in capacitance calculation, which makes the design process more time-efficient.

The outline of the paper is as follows. After a brief introduction of the variable capacitor operation principle, the design methodology will be explained with details in regards to how the formalisms are developed for various types of devices including linear C–V and linear f–V varactors. Next, the accuracies of the designs will be examined through three-dimensional (3-D) finite-element analysis (FEA). Finally, effects of fabrication errors to the characteristics of the designed devices will be presented.

2 Design method

2.1 Operation principle

A typical variable capacitor with comb-drive actuators is composed of two parts as illustrated in Fig. 1, i.e. a sense and a drive capacitor. The former is the actual capacitor component of a main circuit, and its capacitance is

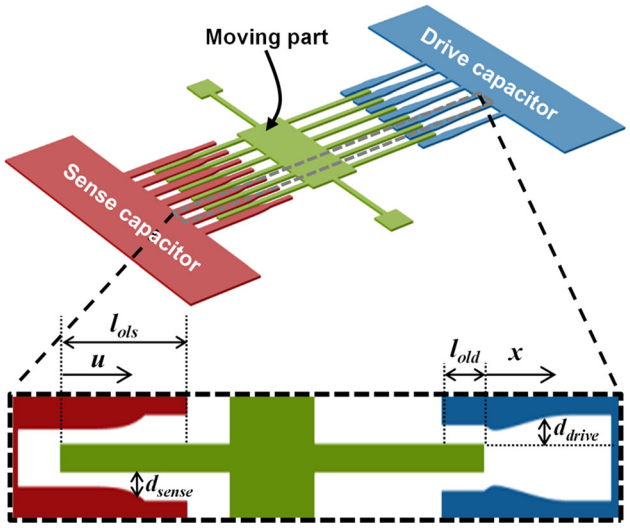

Fig. 1 Schematic diagram of a variable capacitor with shaped-finger comb-drive actuators. The magnified part includes two units of the sense capacitor and two units of the drive capacitor. A linear C–V device with a shaped-finger sense capacitor (n = 5) is shown as an example (color online)

controlled by the latter. When the drive capacitor is not actuated, i.e. when the voltage on it is zero, the fingers of the sense capacitor are most deeply engaged as illustrated in Fig. 1. When a voltage is applied to the drive capacitor, its moving fingers are drawn to its fixed fingers, which makes the moving fingers of the sense capacitor pulled away from the fixed fingers of the sense capacitor so as to decrease the sense capacitance. In a conventional variable capacitor with constant-finger-gap comb-drive actuators, the capacitance–displacement (C–x) relationship is almost linear (Tang et al. 1989). However, the capacitance–voltage (C–V) relationship becomes nonlinear because the electrostatic force is proportional to square of the applied voltage while the mechanical restoring force of a spring is proportional to the displacement for small deformation. In the newly proposed design (Fig. 1), the drive capacitor employs shaped fingers in order to achieve linear C–V characteristics while the sense capacitor is either with constant finger gaps or with shaped fingers. In addition, a device for linear frequency–voltage (f–V) characteristics in VCO circuits will be designed as well. The details of the design procedures will be explained in the following sections.

2.2 Linear C–V device

The design goal, i.e. a linear C–V relationship in the sense part of a device depicted in Fig. 1 can be expressed by the following equation.

$$\frac{dC_{SENSE}}{dV} = c_{CV} \tag{1}$$

$C_{SENSE}(x)$ is the unit 3-D capacitance of the sense capacitor, which is approximated as an integral of 2-D cross-sectional capacitances (C_{sense}) along the length direction x as expressed by (2).

$$C_{SENSE}(x) = \int_{x}^{l_{ols}} C_{sense}(u)du \tag{2}$$

The accuracy of this approximation is examined later in the Sect. 3. A unit capacitance is contributed by a half of a moving finger and a half of a fixed finger—in Fig. 1, a magnified part includes two units of the sense capacitor and two units of the drive capacitor. x is the displacement of the moving part, and u is measured from the tip of the sense moving finger as fabricated (Fig. 1). l_{ols} is the length of the finger overlap on the sense part as fabricated. c_{CV} is a linearity constant, decided by the maximum and the minimum values of C_{SENSE} and V of consideration as follows.

$$c_{CV} = -\frac{C_{SENSE,max} - C_{SENSE,min}}{V_{max} - V_{min}} \tag{3}$$

The maximum and the minimum values of C_{SENSE} ($C_{SENSE,max}$ and $C_{SENSE,min}$, respectively) depend on the finger geometries of the sense capacitor and the boundaries of the region of interest for the moving finger translation, i.e. the initial displacement x_i and the final displacement x_f. It will be explained later the reason why x_i has to be nonzero—and hence, why V_{min} is not zero—in this device. The maximum and the minimum values for V (V_{max} and V_{min}, respectively) are decided by the spring constant k_s, geometries of the drive-comb fingers, and the displacements x_i and x_f. The equilibrium condition between the electrostatic force of the drive capacitor and the restoring force of the springs can be expressed by (4).

$$\frac{1}{2} \times 2N_f \frac{\partial C_{DRIVE}}{\partial x}[V(x)]^2 - k_s x = 0 \tag{4a}$$

$$C_{DRIVE}(x) = \int_{-l_{old}}^{x} C_{drive}(x)dx \tag{4b}$$

$$N_f[V(x)]^2 C_{drive}(x) - k_s x = 0 \tag{4c}$$

$C_{DRIVE}(x)$ is the unit 3-D capacitance of the drive capacitor, which, again, is modeled by a 2-D slice approximation. $C_{drive}(x)$ is the unit 2-D capacitance of the drive capacitor; N_f the number of fingers; and l_{old} the length of the finger overlap on the drive part as fabricated (Fig. 1). By differentiating (4c) with respect to x, and by rearranging the resulting differential equation, one can obtain,

$$\frac{dC_{drive}}{dx} = C_{drive}(x)\left[\frac{1}{x} - \frac{2}{V(x)}\frac{dV}{dx}\right]. \tag{5}$$

By introducing (1) and (4c) to (5), the following governing equation is obtained.

$$\frac{dC_{drive}}{dx} = C_{drive}(x)\left[\frac{1}{x} + \sqrt{\frac{4N_f C_{drive}(x)}{c_{CV}^2 k_s x}}C_{sense}(x)\right] \tag{6}$$

Since (6) is a nonlinear differential equation, the Euler's method is used to find an approximate solution as in previous reports (Hah 2017, 2018a). In this method, a series of $C_{drive,m}$ is calculated by the following approximation with initial conditions of $x_0 = x_i$ and $C_{drive,0} = C_{drive}(x_i)$. m is an index of the series, and h is the uniform step size in x.

$$C_{drive,m+1} = C_{drive,m} + h \cdot \left.\frac{dC_{drive}}{dx}\right|_{x=x_m} \tag{7a}$$

$$C_{drive}(x_m) = C_{drive,m} \tag{7b}$$

$$x_m = h \cdot m \tag{7c}$$

In this work, the conformal mapping method is utilized to calculate both C_{sense} and C_{drive}, with the following equations (Johnson and Warne 1995).

$$C_{sense} \text{ or } C_{drive} = \varepsilon_0\left\{\frac{T_f}{d_f} + \frac{K[\sin(B)]}{K[\cos(B)]}\right\} \tag{8a}$$

$$K(\eta) = \int_0^{0.5\pi} \frac{d\theta}{\sqrt{1 - \eta^2 \sin^2\theta}} \tag{8b}$$

$$B = \frac{\pi W_f}{2(W_f + d_f)} \tag{8c}$$

T_f is the finger thickness (see Fig. 2a); d_f the finger gap; W_f the finger width; ε_0 vacuum permittivity; and $K(\eta)$ the complete elliptic integral of the first kind. By employing the conformal mapping method, the whole design procedure becomes almost all-analytical, minimizing the need to use time-consuming numerical analysis methods. The design parameters used in this work are summarized in Table 1. In (8), approximation is used in the calculation of the fringe field (Johnson and Warne 1995). Therefore, 2-D capacitances were calculated and compared between the conformal mapping method (Fig. 2b) and numerical simulation (Fig. 2c, COMSOL Multiphysics®) for a range of finger dimensions, in order to examine the accuracy of such approximation. It can be seen that the two results are very close to each other. A more precise comparison can be undertaken by examining Fig. 2d, where the % difference is calculated between the two results. It shows that the difference can be quite small (less than 1%) when all the finger parameters (thickness T_f, width W_f, and gap d_f) are comparable to one another. The difference increases as the parameters start to deviate away from one another. It increases significantly for small finger width and large finger gap. It is also interesting to learn that there seems to be a certain condition among the finger parameters where the results from two methods become equal to each other. This condition exists where it looks the surface is folded on

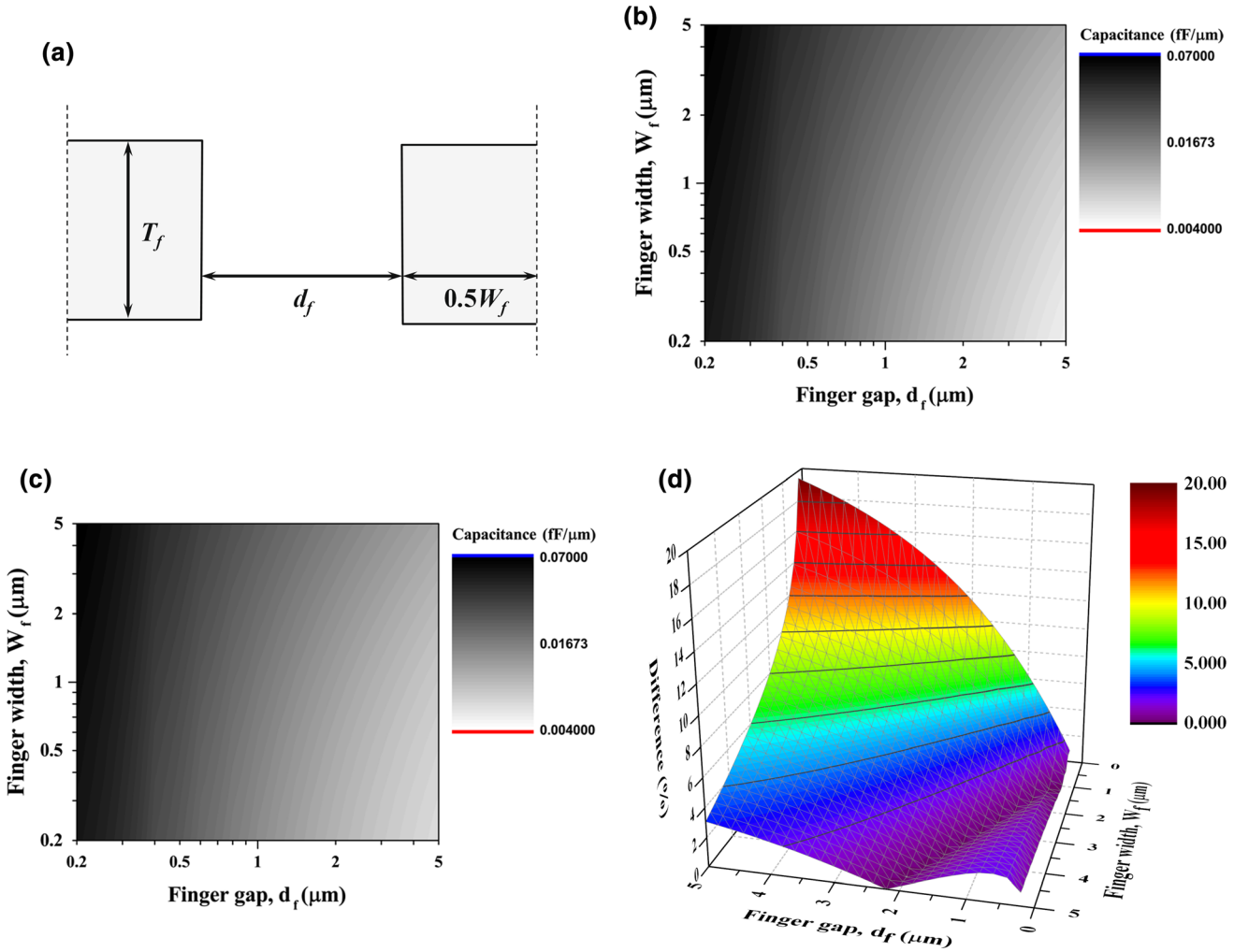

Fig. 2 **a** Definitions of comb-drive finger geometries in a cross-section view of fingers. **b**, **c** 2-D capacitance calculated, **b** by conformal mapping method, and **c** by numerical simulation (COMSOL Multiphysics®). T_f = 1 μm. Shades in a logarithmic scale. **d** % difference between the two capacitance calculation methods (color online)

Table 1 Design parameters

Description	Symbol	Value
Number of fingers	N_f	100
Period of fingers		8 μm
Moving finger width[a]	W_f	2 μm
Drive finger gap at x_i	d_{drive} (x_i)	1 μm
Drive finger gap at x_f	d_{drive} (x_f)	2 μm
Finger travel limit	x_f	20 μm
Spring constant	k_s	0.1 N/m
Inductance for VCO	L	30 nH

[a]Except for the sense finger of a constant-gap sense capacitor device where it is 3 μm

the plot—this is because the difference is calculated as an absolute value.

In the derivation of the formalism, it is assumed that the displacement of the actuator in directions other than x is negligible. One of the main causes which can incur significant conflict to such an assumption is the well-known levitation phenomenon in comb-drive actuators (Tang et al. 1992). This phenomenon is caused by asymmetric electric field in the vertical direction due to a substrate electrode closely placed underneath the actuator. It results in upward motion of the actuator. This levitation can be minimized by increase of separation between the actuator and the substrate, by removal of the substrate underneath the actuator area, or by alternating hot and cold electrodes (Tang et al. 1992). In this work, it is assumed that the substrate is removed underneath the actuator.

2.2.1 Constant-gap sense capacitor

For the sense capacitor, it is both possible to design it with a constant finger gap or to make it with varying gaps. In this subsection, a device with constant-gap sense fingers will be presented. Design with the varying-gap sense fingers will be explained in the following subsection.

One of the things that need to be considered in the design process by using (6) is that there exists no solution at x = 0. Therefore, in order to realize linear C–V characteristics for the entire range of operation, it is inevitable to exclude a region near x = 0 from the region of interest. In other words, an offset voltage is needed at the drive capacitor to shift the region of operation out of small x. The next question is how wide such an excluded-zone should be. To understand that, the optimum drive finger gaps d_{drive} were calculated using (6) for different widths of excluded-zone (x_i), and presented in Fig. 3. The finger gaps d_{drive} at both ends of region of interest (x_i and x_f) were fixed as 1 μm and 2 μm, respectively. It can be learned from the results that for a small value of x_i (less than about 3 μm), there is a part where the optimum finger gaps have to become narrower than the gap at $x = x_i$, i.e. 1 μm. This becomes an issue in relation to the fabrication, i.e. it takes much more efforts to fabricate narrower gaps. To the contrary, for larger values of x_i, the optimum finger gaps can remain wider than the gap at $x = x_i$ for the entire length. Another issue in the case of a small value of x_i is the changing rate of the finger gap, which is high enough near x_i to result in severe field-crowding around that region, making the 2-D slice approximation less accurate. A drawback of the design with large x_i, on the other hand, is a smaller tuning ratio due to narrower region of operation. Considering these trade-offs, 3 μm is considered to be an optimum value for x_i for the linear C–V devices with constant-gap sense capacitors.

Once the optimum C_{drive} is calculated from (6) as a function of x, d_{drive} is calculated back by using (8). Figure 4 presents the calculated C_{SENSE}-V with the optimized finger design. For comparison, the curve of a conventional constant-gap design is also included. For clearer comparison, both the capacitance values and the voltage values are normalized with respect to the maximum and the minimum values for each cases. As expected, the linearity factor (LF)—calculated as the maximum deviation (%) from a straight line—is significantly improved from 49.9% of the conventional constant-gap design to 0.4% of the shaped-finger design. In order to present the difference between a meticulous design and a simple intuitive design, Fig. 4 also includes C–V characteristics from a device with a constant-gap sense capacitor and a linearly-increasing-gap drive capacitor. It is shown that its linearity is improved compared to the conventional device but still significantly worse than that of the proposed device.

2.2.2 Shaped-finger sense capacitor

It is possible to have a varying gap not only for the drive capacitor but also for the sense capacitor to expand the design window. It is apparent that the finger shape of the drive capacitor is determined by that of the sense capacitor. Since the accuracy of the 2-D slice approximation depends on the finger shapes, the actual linearity calculated via 3-D FEA must be affected by the finger shapes. To examine such effects, several profiles were chosen for the sense comb fingers as listed in Table 2 and depicted in Fig. 5a. In the definition of the profile, n means the order of

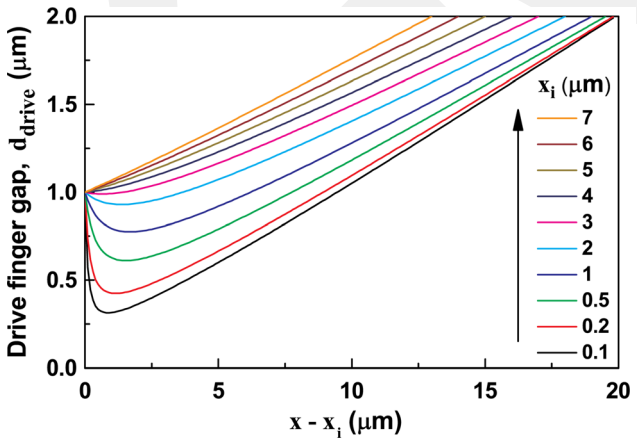

Fig. 3 Effect of excluded-zone widths x_i to the designed drive finger gaps d_{drive} in the linear C–V design with constant-gap sense capacitors. T_f = 10 μm (color online)

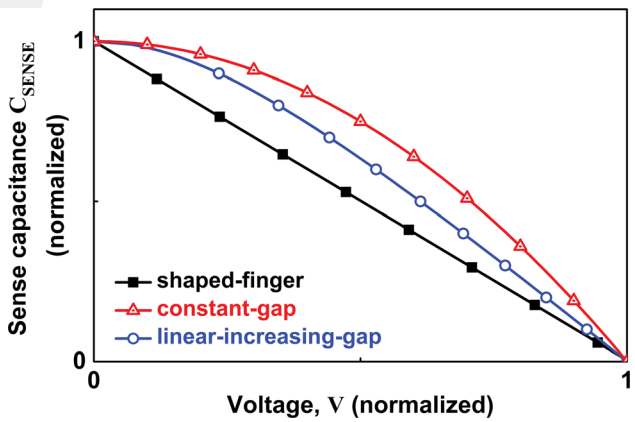

Fig. 4 Calculated sense capacitance vs. voltage applied for the shaped-finger design (linear C–V, constant-gap sense capacitor, T_f = 10 μm, x_i = 3 μm). 2-D slice approximation. Capacitance and voltage values are normalized. C–V characteristics for the devices with constant-gap and the linearly-increasing-gap drive capacitor are plotted as well for comparison (color online)

Table 2 Sense capacitor finger gap profile

n, profile dependence order	Finger gap profile d_{sense} (x)
− 1	$d_{sf} - (d_{sf} - d_{si})\frac{x_i(x_f - x)}{x(x_f - x_i)}$
0.5, 1, 2, and 5	$d_{si} + \frac{d_{sf} - d_{si}}{(x_f - x_i)^n}(x - x_i)^n$

d_{si} sense finger gap at x_i, d_{sf} sense finger gap at x_f

dependence of each profile to u. Some profiles (n = − 1 and 0.5) have more rapid gap change at small u while some profiles (n = 2 and 5) have faster gap change at large u. The design process is the same as the one described in the previous section. Figure 5 shows the calculated drive finger gaps for different sense finger gap profiles. Figure 5d presents the finger shapes based on the calculated finger gaps for two units of the sensor capacitors and two units of the drive capacitors. It is interesting to observe that the drive finger gap profiles are not as widely different among themselves as the sense finger gap profiles. There are two immediately noticeable effects of varying finger gaps in the sense capacitor. First, the sense finger gap profile affects the minimum width ($x_{i,min}$) of the excluded-zone without requiring the narrowest drive finger gap to be less than the finger gap at x_i. While $x_{i,min}$ is about 3 μm in the case of constant-gap sense capacitor (n = 0), it is about 1.5 μm for three cases (n = − 1, 0.5 and 1) and 2 μm for n = 2. Reduction in $x_{i,min}$ means increase in the tuning range. Second effect has a higher impact on the tuning range, i.e. the range becomes smaller due to wider sense finger gaps than the constant-gap sense capacitor device. However, the varying-gap sense capacitor design has another positive effect, which is in regards to the linearity. This effect will be discussed in details in Sect. 3.

2.3 Linear f–V device

The design method can be once again modified for a new objective, i.e. linear frequency–voltage (f–V) characteristics in a VCO application. With a conventional constant-finger-gap design, the f–V relationship is even more

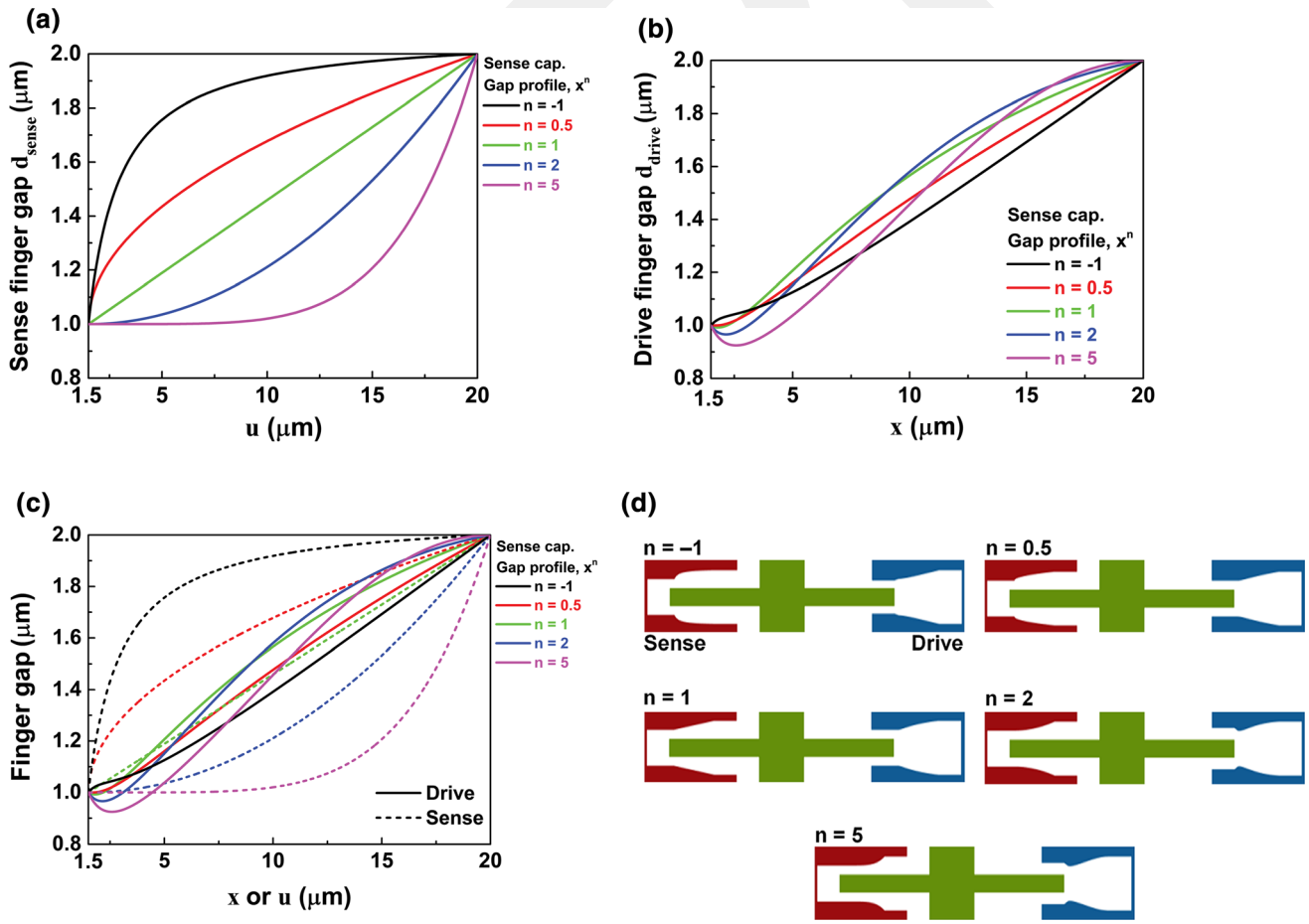

Fig. 5 Design of linear C–V device with shaped-finger sense capacitors. **a** Sense capacitor finger gap profiles, **b** calculated drive finger gaps d_{drive}, **c** coplot of **a** and **b**, and **d** finger shapes (two units, top view). T_f = 10 μm and x_i = 1.5 μm (color online)

nonlinear than the C–V relationship because the electrical resonant frequency is inversely proportional to the square-root of the sense capacitance, as shown by the following equation (Kinget 1999).

$$f(x) = \frac{1}{2\pi}\sqrt{\frac{1}{2N_f L C_{SENSE}(x)}} \tag{9}$$

L is an inductance of an inductor in an LC tank oscillator which is a part of a VCO. The same force balance equation of (4) is used while a new linear constant c_{fV} is defined with a new linearity equation as below.

$$\frac{df}{dV} = c_{fV} = \frac{f(x_f) - f(x_i)}{V(x_f) - V(x_i)} \tag{10}$$

Unlike the case of the linear C–V device, the design of the linear f–V device needs a bit of help from numerical simulation to obtain $C_{SENSE}(x_i)$ in order to calculate $f(x_i)$. Otherwise, the rest of the design process is similar to that of the linear C–V device. The new governing differential equation for the goal of linear f–V design is as follows.

$$\frac{dC_{drive}}{dx} = C_{drive}(x)\left\{\frac{1}{x} + \sqrt{\frac{C_{drive}(x)}{8\pi^2 c_{fv}^2 L x [C_{SENSE}(x)]^3}} C_{sense}(x)\right\} \tag{11}$$

Figure 6 shows the designed drive finger shape d_{drive} for a linear f–V device for several x_i values. In this design, the sense capacitor finger gap was fixed as constant. It is plotted along with the finger shape for the linear C–V design (x_i = 3 μm) for comparison. The corresponding f–V characteristics are provided in Fig. 6c along with those of the conventional constant-finger-gap design. The linear f–V design demonstrates the LF of 0.01% for f–V characteristics, much improved compared to the constant-gap design and the linear C–V design, of which LF are 58.9% and 26.7%, respectively.

Often capacitors are accompanied by inevitable parasitic capacitances (e.g. pad capacitance). In the case of the linear C–V variable capacitor, neither parasitic capacitance of the drive side nor that of the sense side affects the linearity of the device because parasitic capacitances are more or less fixed, and only the capacitance changes are what matters. However, it plays a significant role in the linear f–V device case because a parasitic capacitance affects the resonant frequency of a VCO, and hence its linearity. The following governing differential equation takes the effect of parasitic capacitance (C_p) of the sense side into consideration.

$$\frac{dC_{drive}}{dx} = C_{drive}(x)\left\{\frac{1}{x} + \sqrt{\frac{C_{drive}(x)}{8\pi^2 c_{fv}^2 L x [C_{SENSE}(x) + C_p]^3}} C_{sense}(x)\right\} \tag{12}$$

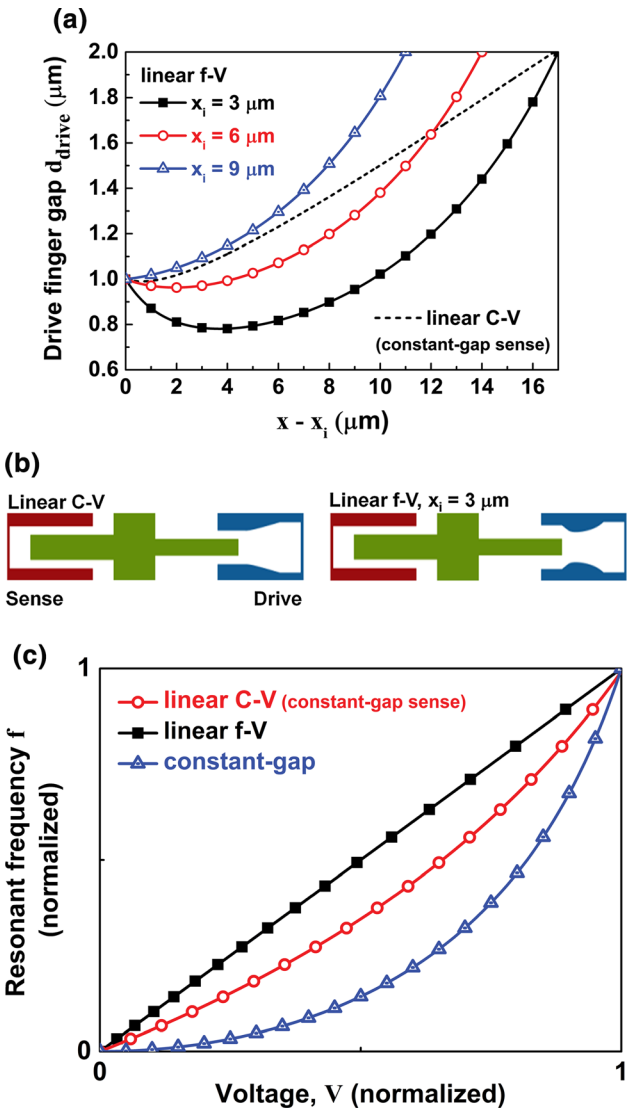

Fig. 6 **a** Calculated drive finger gaps d_{drive} for linear f–V designs. d_{drive} for linear C–V design (x_i = 3 μm) is also plotted for comparison. T_f = 10 μm. **b** Finger shapes (two units, top view) for linear C–V and linear f–V designs. T_f = 10 μm. **c** Calculated resonant frequency of a VCO vs. voltage applied for various designs. Frequency and voltage values are normalized. T_f = 10 μm and x_i = 3 μm (color online)

Linear f–V variable capacitor designs considering parasitic capacitances (C_p) obtained by using (12) are presented in Fig. 7 along with the calculation results. 0.5 pF of C_p is a substantial value considering that the highest sense capacitance in the region of interest is about 0.6 pF. As the parasitic capacitance increases, the drive finger shape change and the drive capacitance change become more moderate (Fig. 7a, b). Figure 7c plots the total sense capacitance ($2N_fC_{SENSE}$) versus drive voltage (offset voltage plus variable control voltage) for different C_p values. In this case, the offset voltage is 5.43 V. Figure 7d

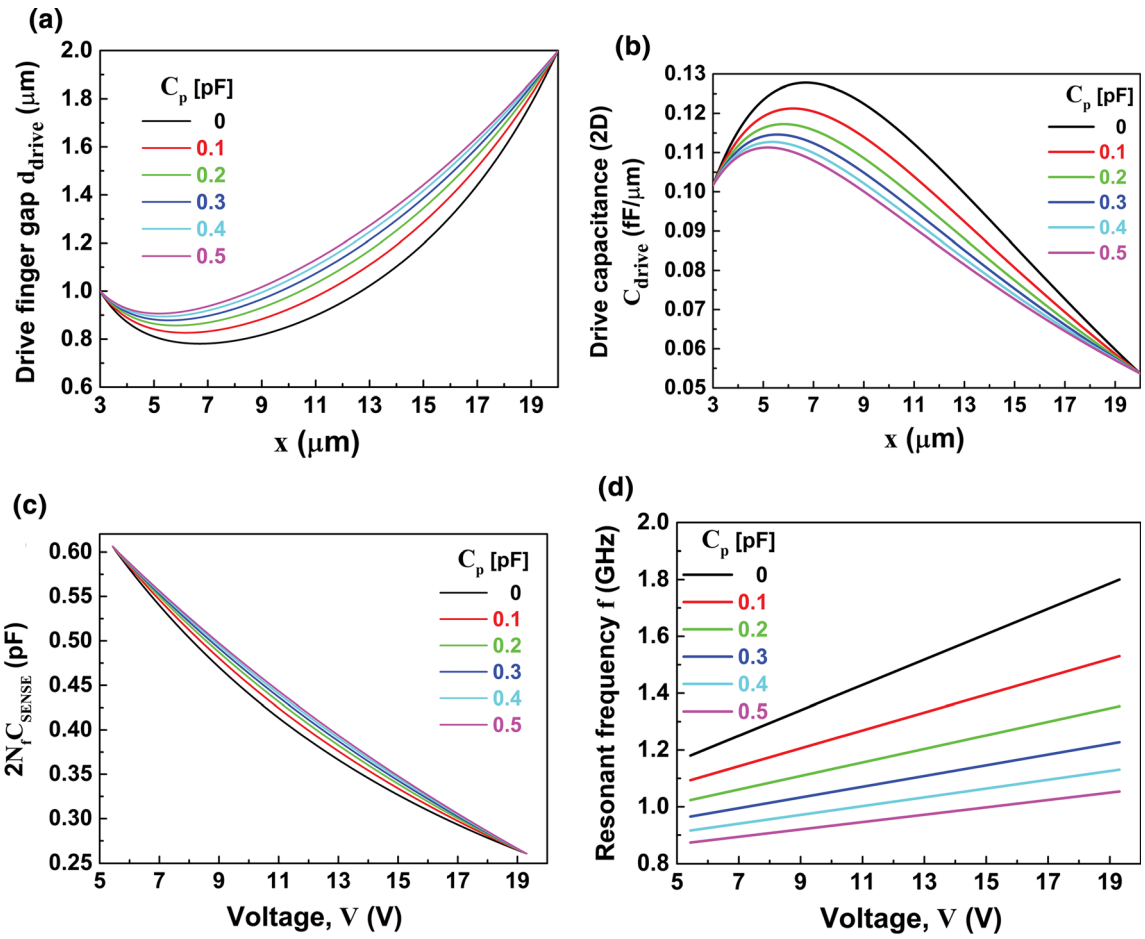

Fig. 7 Effect of parasitic capacitance C_p to finger design and device characteristics in linear f–V devices. Calculated **a** drive finger gaps d_{drive}, **b** drive capacitances C_{drive}, **c** total sense capacitances, $2N_f \times C_{SENSE}$ (excluding C_p), and **d** resonant frequencies f for various parasitic capacitances. T_f = 10 μm and x_i = 3 μm. Only the characteristics between x_i and x_f are plotted. The voltage used in the plot contains both the offset voltage part (5.43 V) and the variable control voltage part (color online)

shows that the resonant frequency becomes lower as C_p increases while good linearity is maintained. It is shown that variable capacitors can be designed for linear f–V characteristics even in the presence of parasitic capacitance once its value is understood.

3 Verification by 3-D finite element analysis

The design method and simulation results described so far are based on a 2-D slice approximation. This implies that the electric field lines are assumed to be orthogonal to the length direction (x-axis). However, in reality, the field lines are not always orthogonal to the length direction when a whole 3-D capacitor structure is considered because of the curved shape of the finger. Moreover, the field lines deviate substantially from the assumed orthogonal ones at the finger tip due to discontinuity of the finger wall and presence of the finger tip wall. In addition, there is the conformal mapping approximation. Therefore, it is necessary to verify the design method through full 3-D simulation (Fig. 8, COMSOL Multiphysics®). Figure 9 shows the C–

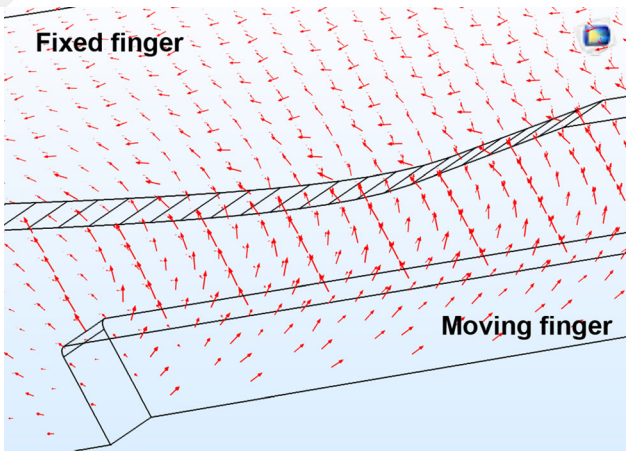

Fig. 8 3-D finite element analysis (COMSOL Multiphysics®) of a device. Arrows indicate the calculated electric fields. A half of a unit is shown for a drive capacitor (color online)

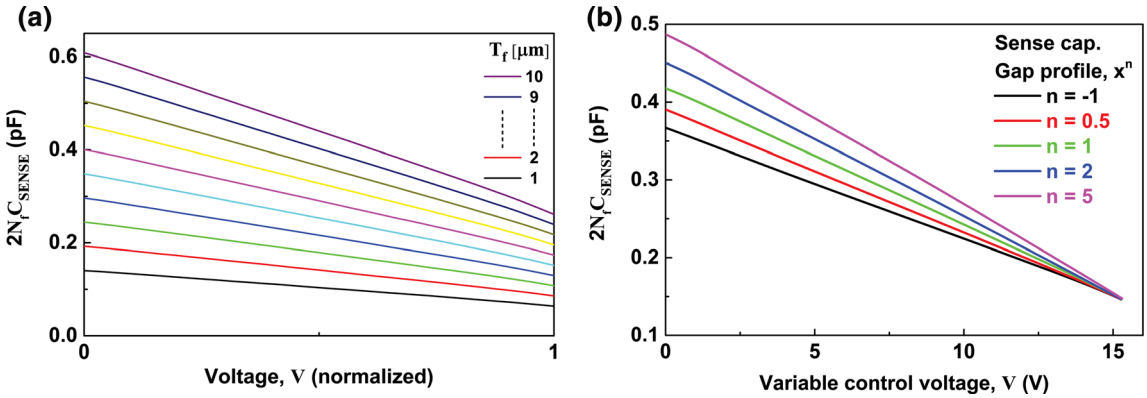

Fig. 9 Total sense capacitance vs. voltage applied, calculated with 3-D finite element analysis for linear C–V designs. **a** Constant-gap sense capacitor devices; T_f = 1, 2, …, 10 μm, and x_i = 3 μm; voltage normalized. **b** Shaped-finger sense capacitor devices; T_f = 10 μm, x_i = 1.5 μm; plotted against variable control voltage (color online)

V characteristics of the linear C–V devices, designed by using 2-D slice approximation, but calculated by 3-D numerical analysis. Figure 9a shows the 3-D simulation results of the constant-gap sense capacitor devices for various finger heights. The linearity factors (Table 3) are found to be better than 2.62% for the finger heights between 1 and 10 μm. This shows that the proposed device can be designed reasonably well with the 2-D slice approximation. Figure 9b shows the 3-D simulation results of the shaped-finger sense capacitor devices with T_f = 10 μm. Only the variable control voltage part (excluding the offset voltage) on the drive comb is used for the plot for clearer comparison. The linearity factors (Table 4) are found to be better (0.77–1.54%) than that of the constant-gap sensor capacitor device (2.04%) in all gap profiles.

3.1 Effect of etch bias

More often than not, fabricated device geometries deviate from the original designs. One of the most frequently occurring fabrication errors in practice is in the form of etch bias. In this section, the effect of etch bias to the characteristics of a linear C–V device is presented, with a focus to the linearity. Etch bias is defined as the amount of geometrical reduction in a structure from one side when looked from top view. For instance, 100 nm of etch bias results in a final width of 800 nm for a designed width of 1 μm. For simplicity, variation in etch bias along the wafer thickness direction is not considered. Also, in practice, because of various reasons including loading effects, the amount of etch bias varies by location, by the ratio of etched areas to unetched areas, and by the shapes of patterns. For this study, however, it is assumed that the etch bias is uniform for the entire structure. More specifically, the etch bias is considered at the capacitors (both the drive and the sense parts) and at the springs. Positive etch bias windens the finger gap so as to reduce the capacitances, and therefore decrease the electrostatic force and the capacitance tuning range. It also reduces the mechanical restoring force due to narrowing of the spring widths. When both effects are combined, decrease in the mechanical restoring force outruns that of the electrostatic force in the device geometries considered in the current study so that the applied voltages are reduced by etch bias overall.

Table 3 Linearity factor (LF) from 3-D simulation results of linear C–V devices with constant-gap sense capacitors (x_i = 3 μm)

Finger height T_f (μm)	LF (%)	Finger height T_f (μm)	LF (%)
1	2.62	6	1.82
2	2.48	7	2.04
3	2.54	8	1.88
4	2.08	9	1.87
5	1.98	10	2.04

Table 4 Linearity factor (LF) from 3-D simulation results of linear C–V devices with shaped-finger sense capacitors (T_f = 10 μm, x_i = 1.5 μm)

Order n	LF (%)
− 1	1.54
0.5	1.21
1	1.16
2	0.77
5	1.42

Figure 10 presents the effect of etch bias to the C–V characteristics of a constant-gap sense capacitor device, examined through 3-D FEA study. Once again, the variable drive voltages are used for the plot. From the results, it can be learned that the sense capacitances and applied voltages are reduced by etch biases as expected. Interestingly,

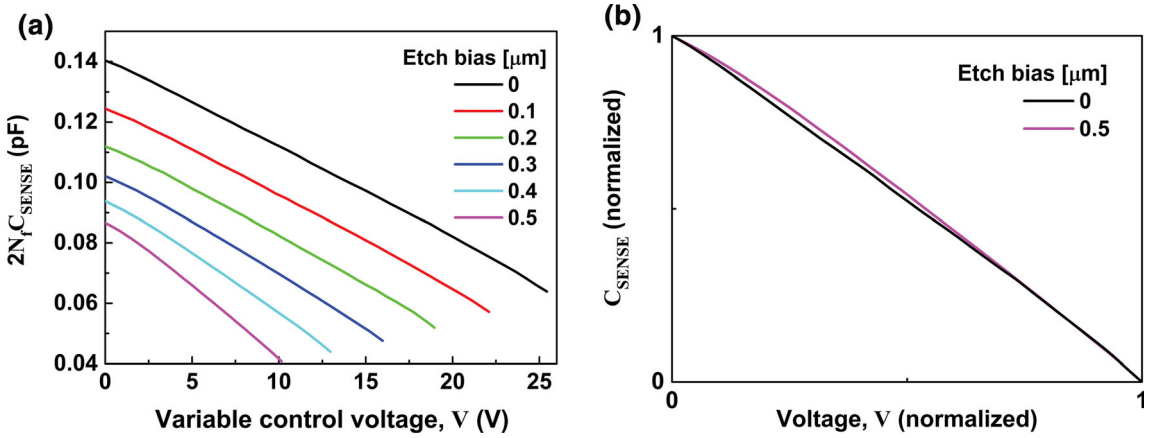

Fig. 10 Effect of etch bias to a linear C–V device with a constant-gap sense capacitor. **a** Calculated C–V characteristics via 3-D FEA analysis for various etch bias amounts. Total sense capacitance is plotted against variable control voltage. **b** C–V characteristics normalized by maximum and minimum values for selected etch biases. T_f = 1 μm and x_i = 3 μm (color online)

linearity of the C–V characteristics is not affected much even with such a high degree of etch bias. To better illustrate the last point, the normalized C–V characteristics are plotted in Fig. 10b for etch bias of 0 and 0.5 μm. It is shown that the curve of 0.5 μm etch bias case almost coincides with that of zero bias after normalization with slight increase in the linearity factor from 2.62 to 3.03%. Therefore, it can be concluded that the major effect of the etch bias to the characteristics of the linear C–V device with a constant-gap sense capacitor is the reduction in sense capacitance and its tuning range.

The effect of etch bias was also examined in the case of a shaped-finger sense capacitor device. The results were similar to those of a constant-gap sense capacitor device. Figure 11a presents an example of normalized C–V characteristics for a device with a sense capacitor of a hyperbolic profile (n = − 1) for etch bias of 0 and 0.5 μm, which looks almost similar to Fig. 10b. Linearity gets worse by etch bias of 0.5 μm to 3.73% from 2.22% of zero etch bias. Figure 11b shows calculated linearity factors with respect to etch bias for various sense capacitor gap profiles including a constant-gap one (n = 0). In all cases, linearity gets worse as etch bias increases although the graphs are not quite monotonous. Aggravation of linearity by etch bias was found to be more in the case of a shaped-finger sense capacitor device although the degree of aggravation was still small.

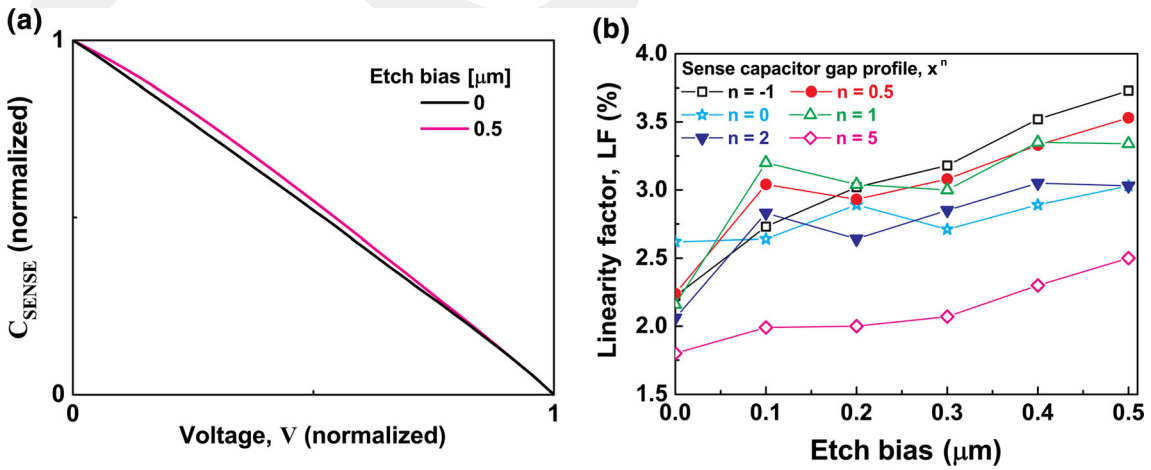

Fig. 11 Effect of etch bias to a linear C–V device with a shaped-finger sense capacitor. **a** Calculated C–V characteristics (profile dependence order n = –1) via 3-D FEA analysis, normalized by maximum and minimum values. T_f = 1 μm and x_i = 2 μm. **b** Effect of etch bias to linearity factors LF for various sense capacitor gap profiles. T_f = 1 μm; x_i = 3 μm for n = 0; x_i = 2 μm for n ≠ 0 (color online)

4 Conclusion

An all-analytical design method was proposed for variable capacitors with linear C–V or linear f–V characteristics, based on the shaped-finger comb-drive actuators. In terms of the sense capacitors, both the constant-gap combs and the shaped-finger combs were considered for the design. 3-D numerical analysis showed that the designed variable capacitors can demonstrate linearity as good as 0.77% in C–V characteristics. It was learned that etch bias does not significantly affect the linearity of the designed devices. The new design method can be extended to various applications where comb-drive actuators are to be designed to achieve specific characteristics.

Acknowledgements This work was partially supported by Research Fund of the Abdullah Gül University (Project Number: FOA-2016-49).

References

Abbaspour-Tamijani A, Dussopt L, Rebeiz GM (2003) Miniature and tunable filters using MEMS capacitors. IEEE Trans Microwave Theory Tech 51:1878–1885. https://doi.org/10.1109/TMTT.2003.814317

Afrang S, Mobki H, Sadeghi MH, Rezazadeh G (2015) A new MEMS based variable capacitor with wide tunability, high linearity and low actuation voltage. J Microelectron 46:191–197. https://doi.org/10.1016/j.mejo.2014.11.006

Baek DH, Eun Y, Kwon DS, Kim MO, Chung T, Kim J (2015) Widely tunable variable capacitor with switching and latching mechanisms. IEEE Electron Device Lett 36:186–188. https://doi.org/10.1109/LED.2014.2378272

Baghelani M, Ghavifekr HB (2017) A novel technique for design of ultra high tunable electrostatic parallel plate RF MEMS variable capacitor. Sens Imaging 18:28. https://doi.org/10.1007/s11220-017-0180-9

Bakri-Kassem M, Mansour RR (2009) Linear bilayer ALD coated MEMS varactor with high tuning capacitance ratio. J Microelectromech Syst 18:147–153. https://doi.org/10.1109/JMEMS.2008.2008626

Borwick RL, Stupar PA, DeNatale JF, Anderson R, Erlandson R (2003) Variable MEMS capacitors implemented into RF filter systems. IEEE Trans Microwave Theory Tech 51:315–319. https://doi.org/10.1109/TMTT.2002.806519

Dec A, Suyama K (2000) Microwave MEMS-based voltage-controlled oscillators. IEEE Trans Microwave Theory Tech 48:1943–1949. https://doi.org/10.1109/22.883875

Elshurafa AM, Ho PH, Salama KN (2012) Low voltage RF MEMS variable capacitor with linear CV response. Electron Lett 48:392–393. https://doi.org/10.1049/el.2011.3340

Engelen JBC, Abelmann L, Elwenspoek MC (2010) Optimized comb-drive finger shape for shock-resistant actuation. J Micromech Microeng 20:105003. https://doi.org/10.1088/0960-1317/20/10/105003

Feng Z, Zhang H, Gupta KC, Zhang W, Bright VM, Lee YC (2001) MEMS-based series and shunt variable capacitors for microwave and millimeter-wave frequencies. Sens Actuators A Phys 91:256–265. https://doi.org/10.1016/S0924-4247(01)00595-7

Hah D (2017) A design method of comb-drive actuators for linear tuning characteristics in mechanically tunable optical filters. Microsyst Technol 23:3835–3842. https://doi.org/10.1007/s00542-015-2736-8

Hah D (2018a) C-band optical filters with micromechanical tuning. Microsyst Technol 24:551–560. https://doi.org/10.1007/s00542-017-3576-5

Hah D (2018b) Analytical design of linear variable capacitors with shaped-finger comb-drive actuators. In: Proc Int symp design, test, integration & packaging of MEMS and MOEMS, pp 163–167. https://doi.org/10.1109/dtip.2018.8394217

Han CH, Choi DH, Yoon JB (2011) Parallel-plate MEMS variable capacitor with superior linearity and large tuning ratio using a levering structure. J Microelectromech Syst 20:1345–1354. https://doi.org/10.1109/JMEMS.2011.2167657

Ikehashi T, Ogawa E, Yamazaki H, Ohguro T (2007) A 3 V operation RF MEMS variable capacitor using piezoelectric and electrostatic actuation with lithographical bending control. In: Int solid-state sensors, actuators and microsystems conf, transducers 2007, pp 149–152. https://doi.org/10.1109/sensor.2007.4300093

Jensen BD, Mutlu S, Miller S, Kurabayashi K, Allen JJ (2003) Shaped comb fingers for tailored electromechanical restoring force. J Microelectromech Syst 12:373–383. https://doi.org/10.1109/JMEMS.2003.809948

Johnson WA, Warne LK (1995) Electrophysics of micromechanical comb actuators. J Microelectromech Syst 4:49–59. https://doi.org/10.1109/84.365370

Kawakubo T, Nagano T, Nishigaki M, Abe K, Itaya K (2006) RF-MEMS tunable capacitor with 3 V operation using folded beam piezoelectric bimorph actuator. J Microelectromech Syst 15:1759–1765. https://doi.org/10.1109/JMEMS.2006.885985

Kinget P (1999) Integrated GHz voltage controlled oscillators. In: Sansen W, Huijsing J, van de Plassche RJ (eds) Analog circuit design. Springer, Berlin, pp 353–381

Lee KB, Lin L, Cho YH (2008) A closed-form approach for frequency tunable comb resonators with curved finger contour. Sens Actuators A Phys 141:523–529. https://doi.org/10.1016/j.sna.2007.10.004

Mahmoodnia H, Ganji BA (2013) A novel high tuning ratio MEMS cantilever variable capacitor. Microsyst Technol 19:1913–1918. https://doi.org/10.1007/s00542-013-1835-7

Moreira EE, Cabral J, Gaspar J, Rocha LA (2016) Low-voltage, high-tuning range MEMS variable capacitor using closed-loop control. Procedia Eng 168:1551–1554. https://doi.org/10.1016/j.proeng.2016.11.458

Nguyen HD, Hah D, Patterson PR, Chao R, Piyawattanametha W, Lau EK, Wu MC (2004) Angular vertical comb-driven tunable capacitor with high-tuning capabilities. J Microelectromech Syst 13:406–413. https://doi.org/10.1109/JMEMS.2004.828741

Nieminen H, Ermolov V, Silanto S, Nybergh K, Ryhanen T (2004) Design of a temperature-stable RF MEM capacitor. J Microelectromech Syst 13:705–714. https://doi.org/10.1109/JMEMS.2004.832192

Pu SH, Darbyshire DA, Wright RV, Kirby PB, Rotaru MD, Holmes AS, Yeatman EM (2016) RF MEMS zipping varactor with high quality factor and very large tuning range. IEEE Electron Device Lett 37:1340–1343. https://doi.org/10.1109/LED.2016.2600264

Reinke J, Fedder GK, Mukherjee T (2010) CMOS-MEMS variable capacitors using electrothermal actuation. J Microelectromech Syst 19:110–1115. https://doi.org/10.1109/JMEMS.2010.2067197

Seok S, Choi W, Chun K (2002) A novel linearly tunable MEMS variable capacitor. J Micromech Microeng 12:82–86. https://doi.org/10.1088/0960-1317/12/1/313

Tang WC, Nguyen TCH, Howe RT (1989) Laterally driven polysilicon resonant microstructures. Sens Actuators A Phys 20:25–32. https://doi.org/10.1016/0250-6874(89)87098-2

Tang WC, Lim MG, Howe RT (1992) Electrostatic comb drive levitation and control method. J Microelectromech Syst 1:170–178. https://doi.org/10.1109/JMEMS.1992.752508

Xiao Z, Peng W, Wolffenbuttel RF, Farmer KR (2003) Micromachined variable capacitors with wide tuning range. Sens Actuators A Phys 104:299–305. https://doi.org/10.1016/S0924-4247(03)00048-7

Ye W, Mukherjee S, MacDonald NC (1998) Optimal shape design of an electrostatic comb drive in microelectromechanical systems. J Microelectromech Syst 7:16–26. https://doi.org/10.1109/84.661480

Yoon JB, Nguyen CTC (2000) A high-Q tunable micromechanical capacitor with movable dielectric for RF applications. In: Tech dig IEEE int electron devices meeting, pp 489–492. https://doi.org/10.1109/iedm.2000.904362